Section V.D ^{3}He Polarization and Transport

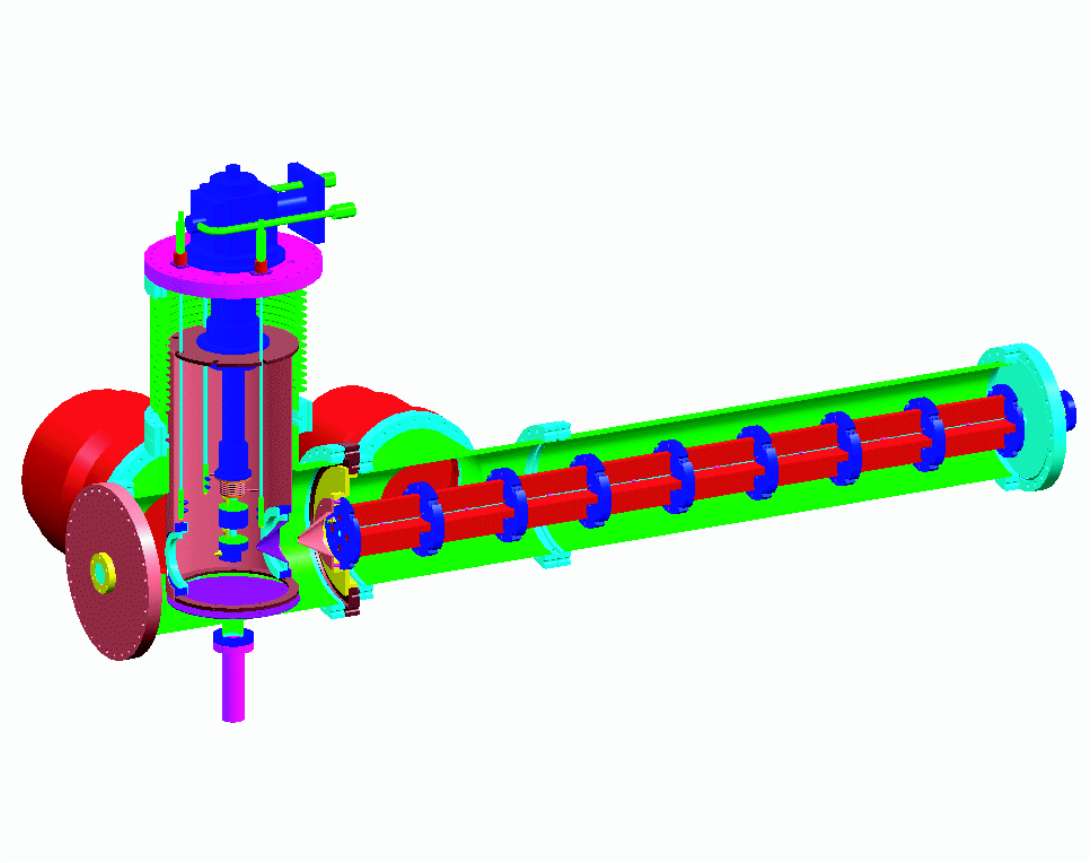

Cutaway view of the polarized ^{3}He source currently under construction at LANL.

As is illustrated in the discussion on sensitivity for the proposed experiment, the purity of the ^{3}He polarization P_3 in the experimental volume is of considerable importance. For a polarized neutron source and $P_3 \approx 1.0$, $\delta f \propto 1/P_3$ where δf is the final uncertainty in the measurement of the possible neutron EDM. However, if the neutron source is unpolarized, the neutron polarization $P_n = \eta P_3$, where η depends on various UCN loss mechanisms, so that $\delta f \propto 1/{P_3}^2$. Moreover, if P_3 and P_n differ from unity significantly, δf depends more strongly on P_3 than $1/{P_3}^2$.

A number of methods have been used in various laboratories to produce polarized ^{3}He [1, 2, 3, 4, 5]. These include melting polarized solid ^{3}He at mK temperatures, optically pumping ^{3}He in the metastable $^3S_1$ state, and using spin-exchange collisions with optically-pumped alkali atoms. The first of these techniques has been used to produce a polarization $P_3 \approx 0.95$, but requires specialized and expensive apparatus. The latter techniques promise polarizations of nearly 90%, but have not demonstrated a polarization exceeding 70% experimentally. The experiment under consideration in this manuscript

would benefit from P_3 greater than has been achieved with these optical pumping methods.

Another method which has the potential to yield a polarization near unity with a simpler apparatus than that of the cryogenic method is to filter an atomic beam of ^{3}He in a magnetic field gradient. While this method is not capable of producing the same quantity of polarized ^{3}He as the previously mentioned methods, the intensity of the polarized beam should be adequate for our purposes.

However, unlike most other atoms that have been polarized in this manner, ground-state ^{3}He has only a nuclear magnetic moment which is smaller than the electron magnetic moment by three orders of magnitude. Due to the relatively small force which can be applied to the ^{3}He through this magnetic moment, the time during which the atom interacts with the field must be increased and the kinetic energy of the atom must be decreased relative to atoms with nonzero electron spin to achieve the same polarization for similar magnetic field gradients. These two requirements can be satisfied by operation of the ^{3}He source at a temperature near 1 K and by use of an interaction region about 1 m long.

V.D.1 Quadrupole Potential

The energy of a magnetic dipole $\vec{\mu}$ in a magnetic field $\vec{B}(\vec{r})$ is given by

$$U(\vec{r}) = -\vec{\mu} \cdot \vec{B}(\vec{r}) \tag{1}$$

and the force imposed on the dipole if the field is static is given by

$$\vec{F}(\vec{r}) = \mu(\hat{s} \cdot \nabla)\vec{B}(\vec{r}) \tag{2}$$

where $\hat{s}$ is the direction of the spin and $|\hat{s}| = 1$. For spin-1/2 ^{3}He, $\mu = -\hbar\gamma_3/2$ where $\gamma_3 = 2.04 \cdot 10^8$/Ts is the ^{3}He gyromagnetic ratio.

We are considering a magnetic quadrupole configuration such as that shown in Fig. 1. This configuration can have a relatively open geometry which helps to remove ^{3}He atoms in the wrong spin state from the interaction region and to reduce the probability that they interact with the atoms confined along the polarizer axis.

However, the magnetic field in the rest frame of an atom will change in magnitude and direction as the atom follows its trajectory through the polarizer. If these changes are too fast, the atom's spin will not maintain its relationship to the magnetic field and the atomic beam will lose polarization. To maintain an atom's polarization throughout its trajectory, its spin must be able to adiabatically follow the direction of the field. Explicitly,

$$\frac{|\dot{B}|}{|B|} \ll |\gamma_3 B|, \tag{3}$$

where $\dot{B} \equiv dB/dt$ and $\gamma_3 B$ is the Larmor frequency.

An additional concern is that the magnitude of the field is theoretically zero at the center of the polarizer. Polarized atoms traveling through this region of zero field may become unpolarized and reduce both the net polarization and polarizer throughput. The

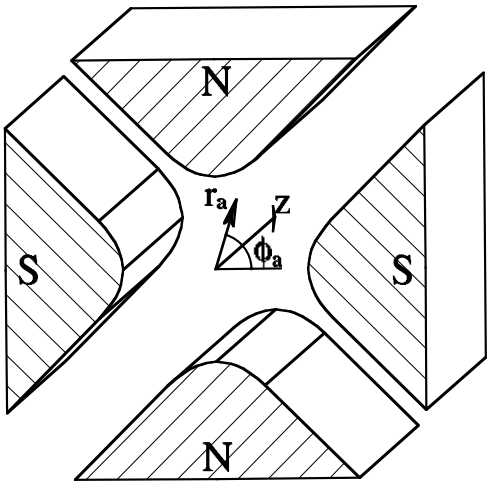

Figure 1: Quadrupole configuration of permanent magnets similar to that being used in the polarizer under construction at LANL.

addition of a weak axial magnetic field B_z mitigates this potential difficulty. If this weak axial field is included, Eq. 3 can be expressed in terms of the velocity of the atom transverse to the axis of the polarizer v_r and the radius of the polarizer aperture R_a as

$$\gamma_3 B_z \gg \frac{|v_r|}{R_a}. \tag{4}$$

As long as this condition is satisfied, an atom's spin will maintain its initial relationship with the magnetic field so that $\hat{s} = \hat{B}$ always. The force from Eq. 2 can then be expressed as

$$\vec{F_B}(\vec{r}) = \pm\mu\frac{B_0}{R_a}\frac{1}{\sqrt{1+(B_z/B_0)^2(R_a/r)^2}}\hat{r} \tag{5}$$

where r is the distance from the axis of the polarizer to the atom, B_0 is the magnitude of the field near the surface of one of the magnets and $\pm$ refers to the two spin states anti parallel and parallel to $\vec{B}$, respectively. Obviously, atoms whose spin is parallel to $\vec{B}$ experience a restoring force and the atoms in the other state are repulsed from the axis of the quadrupole. Note that the depth of the potential well is reduced unless $B_z \ll B_0$.

V.D.2 Polarizer Parameters

If the source is a jet of gaseous ^{3}He some distance from the entrance aperture of the polarizer, the acceptance angle as a function of atom velocity can be estimated by setting the magnetic potential energy equal to the kinetic energy of the transverse motion. Thus,

$$\sin(\theta_0) \approx \sqrt{\frac{\mu B_0}{mv^2}} \tag{6}$$

for an atom located halfway between the center and edge of the polarizer and a magnetic field of $B_0 \gg B_z$ at the edge of the polarizer.

The velocity dependence of the intensity, $I(v)$, of an atomic beam can be expressed as [6]

$$I(v) = I_0 \frac{2}{\alpha^4} v^3 e^{(-v^2/\alpha^2)} \tag{7}$$

where $\alpha^2 = 2k_B T/m$. With $v_{rms} = \sqrt{2}\alpha$ to replace v in Eq. 6, the acceptance angle can be expressed as a function of source temperature T as

$$\sin(\theta_0) \approx \sqrt{\frac{\mu B_0}{4k_B T}}. \tag{8}$$

For $B_0 = 0.75\,\mathrm{T}$ and $T = 0.6\,\mathrm{K}$, this yields $\theta_0 \approx 0.9°$.

Eq. 6 can also be used with Eq. 4 (which also requires that $B_z \ll B_0$) to further constrain B_z. These relationships can be combined to yield

$$\frac{1}{R_a}\sqrt{\frac{\hbar}{2m\gamma_3 B_0}} \ll \frac{B_z}{B_0} \ll 1. \tag{9}$$

For the values of B_0 and T stated previously, $B_z \approx 0.03\,\mathrm{T}$ is an appropriate choice.

V.D.3 Atomic Beam Intensity

The angular dependence of the intensity of an effusing source is given by $dI_0/d\Omega = n\bar{v}A\cos(\theta)/4\pi$ [6] where n and A are the source density and aperture area respectively, θ is the azimuthal angle from the source aperture normal and Ω is the solid angle. Integrating between $0 \le \theta \le \theta_0$ yields

$$\begin{aligned} I_0 &= \frac{1}{4} n\bar{v}A\sin^2(\theta_0) \\ &\approx \frac{1}{2}\frac{p}{\sqrt{mk_BT}} A\sin^2(\theta_0) \\ &\approx \frac{1}{8}\frac{\mu B_0}{\sqrt{m(k_BT)^3}} pA, \end{aligned} \tag{10}$$

where p is the source pressure. For ^{3}He and the parameters discussed above, Eq. 10 yields $I_0/pA \approx 1 \cdot 10^{16}/\mathrm{s{\cdot}mtorr{\cdot}cm^2}$. The design of the source aperture that we are currently considering will allow for an effective area of about $1\,\mathrm{cm}^2$.

The pressure at which the source can be operated depends upon the specific geometry of the source nozzle and there are several concerns that must be addressed to determine an adequate nozzle design. First, the gas pressure in the volume outside the nozzle must be kept much lower than the source pressure. This depends on several items such as the geometry of that volume, the capacity of the pumps acting on that volume and, of course, the flow of ^{3}He from the nozzle. Second, we expect that the amount of ^{3}He in the system will be relatively small and will need to be used efficiently. Fortunately, the forward flow

and hence the quality of the vacuum outside the source can be enhanced by building the aperture from a collection of small tubes of radius ρ_s and length L_s. The forward flow remains the same while the integrated intensity is reduced by $8\rho_s/3L_s$ [6].

A third concern is that the mean-free-path in the nozzle aperture given by $\lambda_s \approx 1/\sqrt{2}n\sigma$, where $\sigma = 1.0 \cdot 10^{-14}\,\mathrm{cm}^2$ is the scattering cross-section of He, should not be much smaller than ρ_s to insure that the lowest velocity atoms are not scattered out of the beam. The mean-free-path for helium can be expressed as $\lambda_3/p \approx 4.4 \cdot 10^{-3}\,\mathrm{cm/mtorr}$. With $\rho_s = 3.5 \cdot 10^{-1}\,\mathrm{mm}$, p should be less than a few $10^{-2}\,\mathrm{mtorr}$ and

$$I_0 \approx 1 \cdot 10^{14}/\mathrm{s}, \tag{11}$$

given that only half of the ^{3}He enter the polarizer in the spin state where $\hat{s} = \hat{B}$.

V.D.4 Numerical Simulations

As noted in [7], the actual performance of the polarizer will differ from the simple calculations of the previous section. This is due in part to the fact that several important considerations were ignored in these simple calculations. For example, we must consider a method to inhibit fast atoms in the wrong spin state from traversing the polarizer and we must consider the mechanical angular momentum of the atom about the axis of the polarizer. In defense of the calculation presented in the previous section, these items are difficult to treat analytically.

That the angular momentum of the ^{3}He about the polarizer axis is likely to be important, can be illustrated by considering the depth of the potential well relative to an atom's kinetic energy. The radial restoring force including the pseudo-force caused by the atom's centripetal acceleration can be expressed as

$$\begin{aligned} \vec{F}(\vec{r}) &\approx -\frac{1}{2}\hbar\gamma_3\frac{B_0}{R_a}\hat{r} + mr_0^2v_\phi^2\frac{1}{r^3}\hat{r} \\ &= (-\alpha + \beta\frac{1}{r^3})\hat{r} \end{aligned} \tag{12}$$

where r_0 and v_ϕ are the initial radial position and polar velocity of the atom. The potential energy is then given by

$$U(r) = \alpha r + \beta\frac{1}{2r^2} \tag{13}$$

which has a minimum at $r^3 = \beta/\alpha$. The potential minimum

$$U_{min} = \frac{3}{2}\alpha^{2/3}r_0^{2/3}(mv_\phi)^{1/3} \tag{14}$$

which depends upon the kinetic energy of the polar motion to the 1/3 power. Clearly, a atom can enter the polarizer with more kinetic energy in the transverse motion than was considered in Eqs. 6 and 8.

V.D.5 Equations of Motion

To better analyze the performance of the polarizer and to investigate several different schemes to inhibit fast atoms from traversing the polarizer in the wrong spin state, we chose a numerical analysis. This analysis involves a Runge-Kutta scheme to integrate the differential equations describing the motion of the atom as it traverses the polarizer.

In addition to the restoring force expressed in Eq. 5, the effects of gravity and of bending the horizontally oriented polarizer guide upwards were included. We also included the ability to simulate the effect of cylindrically symmetric baffles placed along the bore of the polarizer to inhibit fast atoms from traversing it unimpeded.

The effects of gravity and of bending of the polarizer bore can be expressed as

$$\begin{aligned} \vec{F_g} &= -m(g + \frac{v_z^2}{R_p})\hat{y} \\ &= -m(g + \frac{v_z^2}{R_p})(\sin(\phi)\hat{r} + \cos(\phi)\hat{\phi}) \end{aligned} \tag{15}$$

where g is the acceleration due to gravity, v_z is axial velocity of the atom, and R_p is the radius of curvature of the "bent" polarizer. The acceleration due to gravity is about 1% of the acceleration due to the interaction of the dipole and magnetic field, but was included for completeness as it introduced no additional complexity to the calculation.

The equations of motion can be immediately expressed in cylindrical coordinates as

$$\begin{aligned} \vec{F_t} &= \vec{F_B} + \vec{F_g} \\ &= m\ddot{\vec{r}} \\ &= m((\ddot{r} - \dot{r}\dot{\phi}^2)\hat{r} + (r\ddot{\phi} + 2\dot{r}\dot{\phi})\hat{\phi} + \ddot{z}\hat{z}) \end{aligned} \tag{16}$$

Velocities were chosen randomly from a weighted distribution that accurately reproduces Eq. 7. The directions of atoms leaving the source were also made to accurately reproduce the $\cos(\theta)$ dependence of an effusing source and no correction was made to simulate a source aperture of finite length. In all cases except otherwise noted, the simulations were made for a polarizer whose dimensions are those of the polarizer currently under construction at LANL. The relevant dimensions are: source aperture radius $R_s = 6\,\text{mm}$, separation between source aperture and polarizer entrance aperture $s = 22\,\text{cm}$, polarizer aperture (or bore radius) $R_a = 7.5\,\text{mm}$, and polarizer length $L = 1.25\,\text{m}$. The source temperature has been fixed at $T = 0.6\,\text{K}$ and the magnetic fields are assumed to be $B_0 = 0.75\,\text{T}$ and $B_z = 0.03\,\text{T}$ for these simulations.

V.D.6 Straight, Unobstructed Polarizer

Figs. 2 show some results of a simulation for a straight polarizer when $s = R_a$. Only a few percent of the incident atoms would successfully traverse the polarizer in this situation due to the large angle relative to the polarizer axis with which most of them enter the polarizer; 1/4 of the atoms leaving the source enter the polarizer. Of particular significance in these data is Fig. 2(d) which shows the distribution of the angle of incidence for atoms which could successfully traverse the polarizer. The standard deviation of these data

from a mean of $\theta = 0$ is $\sigma_\theta = 1.1°$. This is about 20% larger than $\theta_0 = 0.9°$ from Eq. 8 which better represents a maximum angle than a standard deviation. As mentioned previously, this effect was expected because the simulation treated the transverse motion more accurately than did our previous analysis.

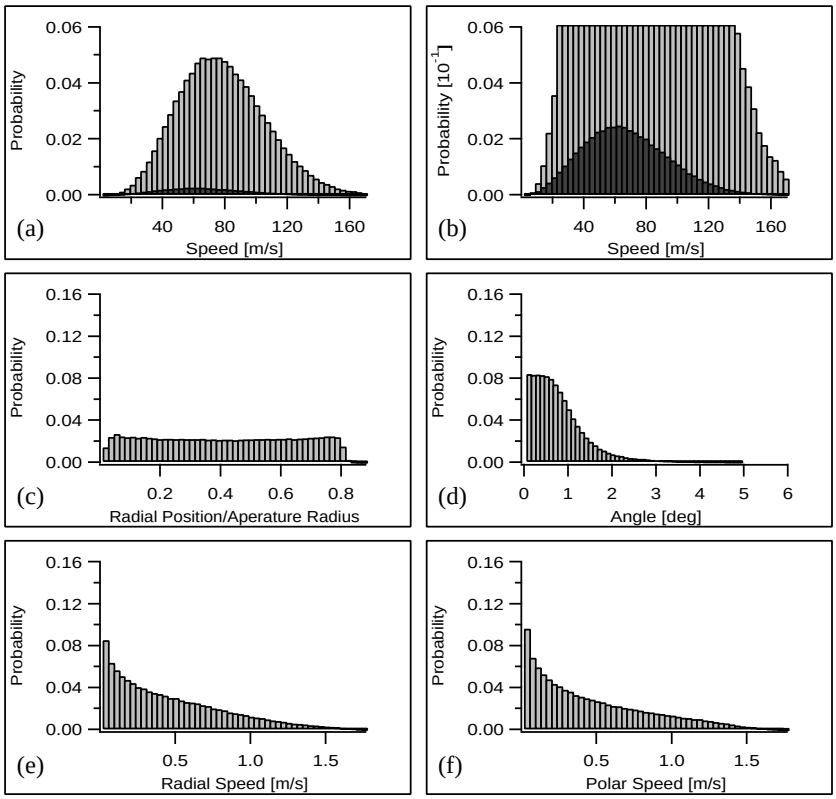

Figure 2: Results of a simulation where $s = R_a$ for atoms with $\hat{s} = \hat{B}$. The polarizer was straight and unobstructed. The light gray bars in (a) represent the velocity distribution of atoms which enter the polarizer and the dark gray represents the subset that successfully traverses the polarizer. Panel (b) shows the same results as (a) with a different vertical scale. Panels (c-f) show the distributions of various initial conditions for atoms which successfully traverse the polarizer. Only 4.8% of the incident atoms travel the full length of the polarizer, but 1/4 of all the atoms leaving the source enter the polarizer. A total of $250,000$ successful traverses of the polarizer were used to generate these histograms.

Figs. 3 show some results of a simulation for a straight polarizer as in Figs. 2, but with the source and polarizer separated by the same distance they will be separated in the device being constructed at LANL. Note that the angular dependence in Fig. 3(d) is slightly different from Fig. 2(d). Also note that the probability is very small for an atom to enter the polarizer along the axis and successfully traverse the polarizer. From

conservation of energy and momentum, we can then determine that it is equally unlikely that an atom will pass through the axis during a successful traverse of the polarizer. Because the atoms do not pass through the center of the polarizer where the transverse magnetic field is null, they will not suffer depolarization by entering a region with an undefined quantization axis even if the additional axial field $B_z = 0$.

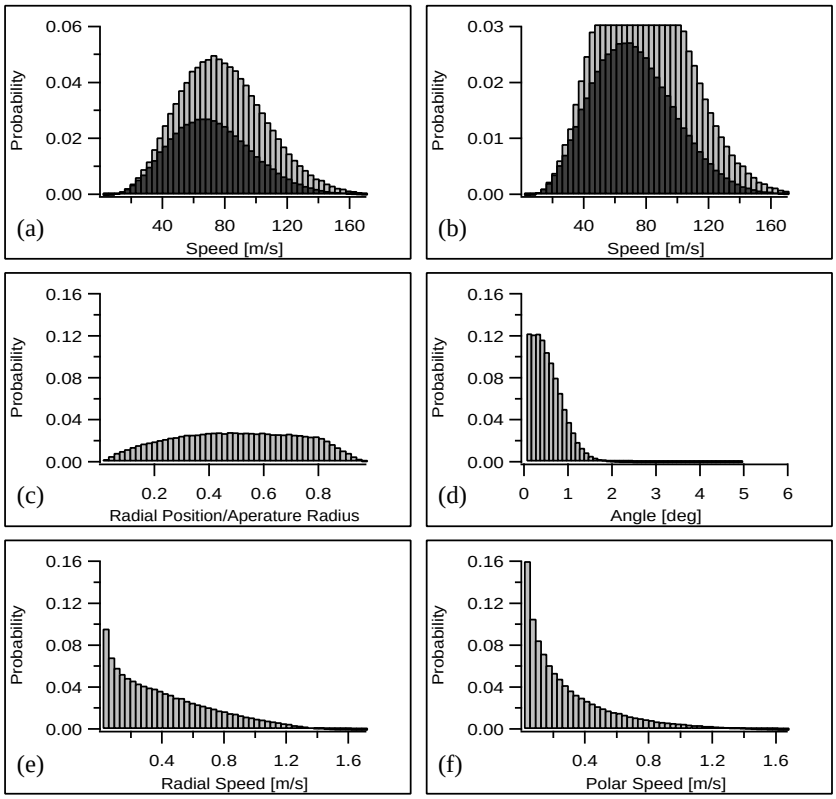

Figure 3: Results of a simulation with a straight polarizer and no obstructions for atoms with $\hat{s} = \hat{B}$. The light gray bars in (a) represent the velocity distribution of atoms which enter the aperture of the polarizer and the dark gray represents the subset that successfully traverses the polarizer. Panel (b) shows the same results as (a) with a different vertical scale. Panels (c-f) show the distributions of various initial conditions for atoms which successfully traverse the polarizer. About 53% of the incident atoms successfully traverse the entire length of the polarizer but only 0.1% of the atoms leaving the source enter the polarizer. A total of $250,000$ successful traverses of the polarizer were used to generate these histograms.

This calculation suggests that the probability of a ^{3}He atom to traverse the polarizer, given that it impinges on the polarizer entrance aperture and $\hat{s} = \hat{B}$, is $P_+ = 0.53$. To calculate the throughput, Eq. 10 can be used where $\sin(\theta_0) \approx R_a/s$. Given that $B_0 = 0.75\,\mathrm{T}$, $T = 0.6\,\mathrm{K}$, $p = 3 \cdot 10^{-2}\,\mathrm{mtorr}$, $A = 1\,\mathrm{cm}^2$ and half of the incident ^{3}He have

$\hat{s} = \hat{B}$

$$I_0 = 4 \cdot 10^{14}/\mathrm{s}, \tag{17}$$

which is four times larger than Eq. 11

The polarization of the ^{3}He can be calculated if the throughput is known for atoms which enter the polarizer in the orthogonal spin state. We have determined that the probability of such an atom to successfully traverse the polarizer is $P_- = 0.0004$. The net polarization can be calculated from

$$P = \frac{P_+ - P_-}{P_+ + P_-}. \tag{18}$$

For $P_+ = 0.53$ and $P_- = 0.0004$ as determined above, $P > 0.998$.

V.D.7 Two Baffles

Figs. 4 show some results of a simulation for a straight polarizer as in Figs. 3, but with two baffles placed in the bore of the polarizer to eliminate line-of-sight down the bore. The configuration of the baffles chosen was a disk-shaped structure placed in the center of the polarizer midway between the ends and a matching washer placed at the exit baffle. In all cases the edges of the baffles would overlap by 0.5 mm if superposed. In this manner, atoms in the wrong spin state should not be able to traverse the polarizer under any circumstances. Several simulations were compared to arrive at the optimum choice for the size of the baffles. A comparison of these results is displayed in Fig. 5 and shows that the optimum radius of the disk baffle is slightly less than half of the radius of the polarizer bore.

The results displayed in Figs. 4 are those for the baffle size with the largest throughput. In this configuration, only 6.6% of the incident atoms in the proper spin state would pass unimpeded through the polarizer. Note the discreet velocities which would traverse the polarizer as shown in Fig. 4(b). Neglecting the effect of the atoms' mechanical angular momentum, these represent atoms whose trajectories would be parabolas and would make an even number of passes through, or nearly through the axis of the polarizer. Obviously, the throughput is dependent on the velocity profile and therefore on the temperature of the source. A warmer source may be more effective for this arrangement. Also note the profile of the angles of incidence in Fig. 4(d) which has a maximum at about 0.7°. This suggests that a different source nozzle geometry with slightly angled capillaries may be able to increase the number of atoms which can pass the baffles undeflected.

V.D.8 Bent Polarizer

Figs. 6 show the results of a simulation for a polarizer bent to prevent a simultaneous view of the entrance and exit apertures down the bore of the polarizer. As in the situation with baffles discussed previously, fast atoms in the wrong spin state should not be able to traverse the polarizer and degrade the polarization of the collected ^{3}He. The radius of curvature was chosen to be $R_p = L^2/16R_a \approx 12\,\mathrm{m}$ where L is the length of the polarizer. As can be seen in Fig. 6(b), this method would clearly favor the slowest atoms;

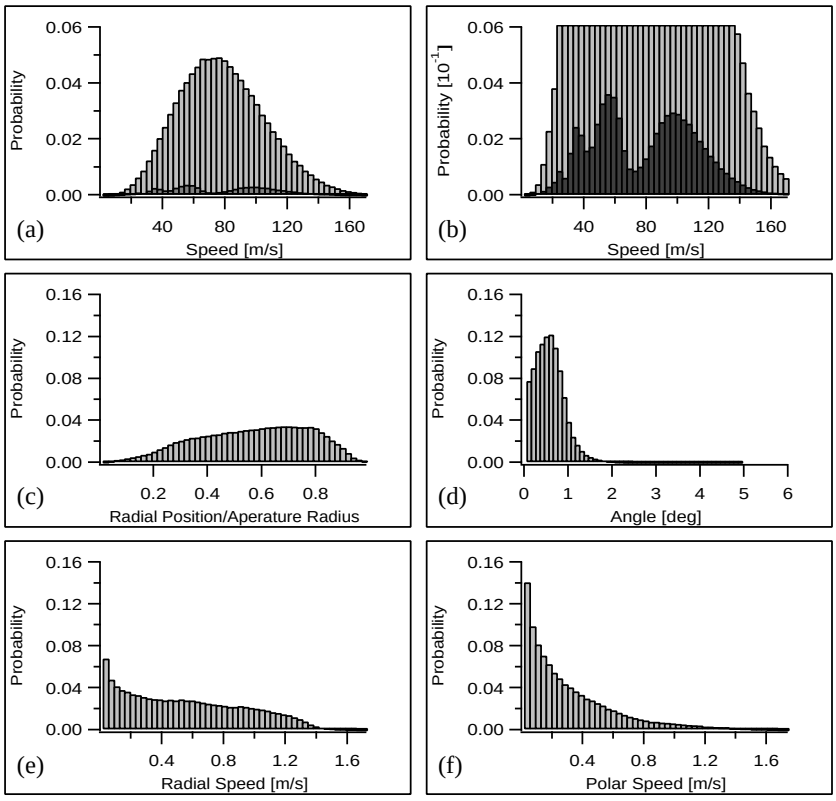

Figure 4: Results of a simulation with a straight polarizer and two baffles along the bore for atoms with $\hat{s} = \hat{B}$. The first baffle is a disk of radius 3.3 mm in the center of the bore and midway between the ends. The second baffle is a washer with opening radius 2.8 mm located in the exit aperture. This configuration was found to optimize the throughput for this size polarizer and source temperature. The light gray bars in (a) represent the velocity distribution of atoms which enter the aperture of the polarizer and the dark gray represents the subset that successfully traverses the polarizer. Panel (b) shows the same results as (a) with a different vertical scale. Panels (c-f) show the distributions of various initial conditions for atoms which successfully traverse the polarizer. About 6.6% of the incident atoms travel the length of the polarizer unobstructed. A total of 250,000 successful traverses of the polarizer were used to generate these histograms.

fast atoms would have enough centripetal acceleration to overcome the restoring effect of the magnetic field. This method would be slightly less effective than using the baffles as described previously, as only about 5.7% of the incident atoms could traverse the polarizer without colliding into the walls or passing out of the bore. If the source is colder than 0.6 K this configuration may have better throughput than the baffle configuration. (We may be able to achieve 0.4 K.)

Unfortunately, neither the baffle nor bent polarizer configurations could allow even

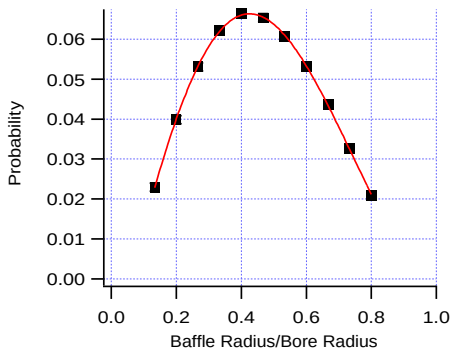

Figure 5: Probability for successfully traversing the polarizer as a function of baffle size for atoms with $\hat{s} = \hat{B}$. The two baffles are 1) a disk-shaped structure placed in the center of the polarizer midway between the ends and 2) a matching washer placed at the exit baffle. The edges of the baffles would overlap by 0.5 mm if superposed. The baffle size reported is the radius of the disk less 0.25 mm.

10% throughput, if the results of these simulations accurately reproduce reality. However, another configuration is suggested by the equation $R_p = L^2/16R_a$, where the radius of curvature depends on the square of the polarizer length. A numerical simulation was performed with a double-length polarizer of 2.5 m and the results were promising. The calculated throughput increased by more than a factor of 4 to 28% or about half of the throughput of a straight polarizer of half the length (and no baffles). The results for optimally chosen baffles of the same configuration used previously, but adapted for the longer polarizer, showed a small decrease in the throughput.

V.D.9 Net Polarization and Throughput for Obstructed and Bent Polarizers

Either the use of baffles or bending the polarizer, to prevent a line-of-sight view of both ends of the polarizer down its bore should prevent any gas which is not ^{3}He in the desired spin state from traversing the polarizer, provided the bore is sufficiently open along its length to allow the escape of this other gas into the surrounding vacuum. However, the highest throughput allowed by either of these methods for $L = 1.25$ m is about 3% of the incident ^{3}He so that $I_0 \approx 5 \cdot 10^{13}$atoms/s. While this flux is theoretically sufficient for the experiment described in this manuscript, we do not feel that it allows a sufficient margin of error; experiments rarely work as well as is theoretically possible.

The "double-length" polarizer with $L = 2.5$ m and a bend of $R_p = L^2/16R_a$ is not an experimentally attractive solution if another solution can be found for $L = 1.25$ m, due to the additional apparatus required and space constraints. More explicitly, we wish to build two identical polarizer sections and connect them with a short section in which an RF field can be applied to change the direction of polarization and investigate the net polarization of the ^{3}He. The length of the entire apparatus would then exceed our

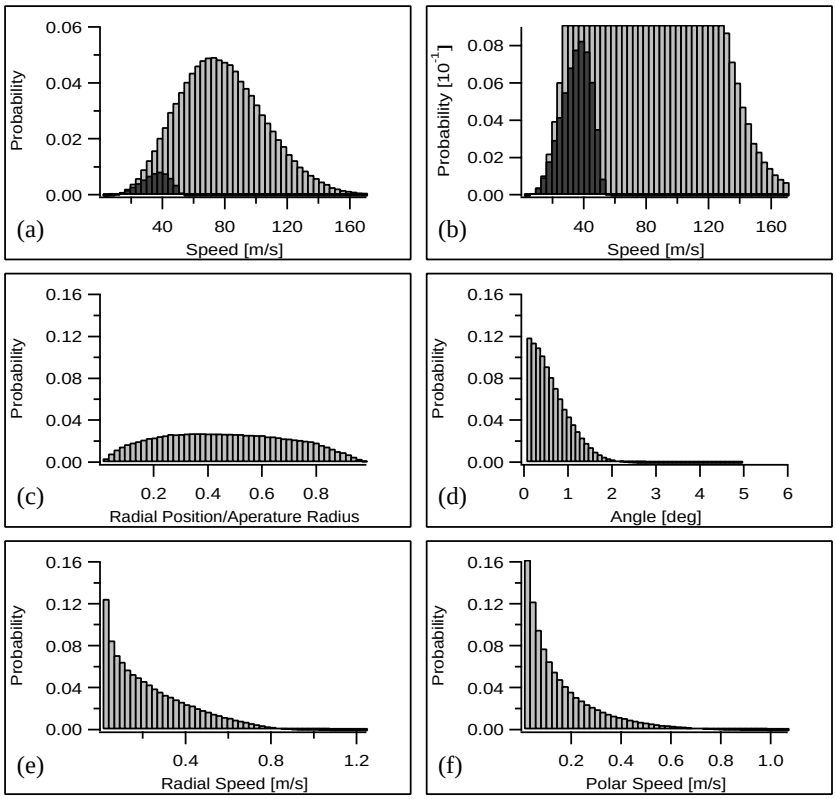

Figure 6: Results of a simulation for a polarizer bent to occlude the view of one aperture from the other looking down the bore and for atoms with $\hat{s} = \hat{B}$. The light gray bars in (a) represent the velocity distribution of atoms which enter the aperture of the polarizer and the dark gray represents the subset that successfully traverses the polarizer. Panel (b) shows the same results as (a) with a different vertical scale. Panels (c-f) show the distributions of various initial conditions for atoms which successfully traverse the polarizer. Only about 5.7% of the incident atoms successfully traversed the polarizer. A total of $250,000$ successful traverses of the polarizer were used to generate these histograms.

currently available space.

V.D.10 Conclusion

In conclusion, it appears that a throughput of about $I_0 \approx 4 \cdot 10^{14}$/s is possible for a polarization of $P > 0.998$ with a polarizer of the type currently being assembled at LANL. It is clear that the straight, unobstructed polarizer configuration is superior to any of the other configurations considered here such as placing a particular series of baffles along the length of the polarizer or a slight bend to occlude a view of one end from the other. Although the polarization is theoretically unity with these other methods, the 0.2% lower polarization with the straight, unobstructed polarizer is insignificant compared with its

tenfold improvement in throughput.

As was suggested previously, the more accurate numerical analysis suggests a four times higher flux than the simple calculation of the first section. A further conclusion, which can be derived from the numerical analysis, is that the axial magnetic field B_z is not required; ^{3}He with $\hat{s} = \hat{B}$, that would successfully traverse the polarizer, would not pass through the axis where the transverse field is null.

References

[1] G.A. Vermeulen and G. Frossati, Cryogenics 27, 139 (1987).

[2] R.G. Milner *et al.*, Nucl. Instrum. Methods Phys. Res. A 274, 56 (1989).

[3] P.J. Nachor *et al.*, J. Physique Lett. 43L, 525 (1982).

[4] C.G. Aminoff *et al.*, Rev. Phys. Appl. 24, 827 (1989).

[5] K.P. Coulter *et al.*, Nucl. Inst. Meth. A 270, 90 (1988).

[6] N.F. Ramsey, *Molecular Beams* (Oxford Univ. Press, Oxford, 1956).

[7] R. Golub and S.K. Lamoreaux, Phys. Reports 237, 1 (1994).